Brazilian Journal of Geophysics, **42** (2024), 1, 1–12
Brazilian Geophysical Society
ISSN 2764-8044
DOI 10.22564/brjg.v42i1.2309

QUANTIFYING ANISOTROPY PARAMETERS IN WEAKLY ANISOTROPIC MEDIA THROUGH DIFFRACTION TRAVELTIME PARAMETER CLUSTERS

Tiago Antonio Alves Coimbra [1*], Rodrigo Bloot [2], Alexandre William Camargo [1], and Jorge Henrique Faccipieri Junior [1]

[1]Universidade de Campinas - Unicamp, HPG / Cepetro, Campinas, SP, Brazil
[2]Universidade Federal da Integração Latino-Americana – Unila, Foz do Iguacu, PR, Brazil

*Corresponding author: tgo.coimbra@gmail.com

ABSTRACT. The seismic response datasets obtained from anisotropic media present several challenges for established seismic processing methods. To determine whether wavefront interference stems from anisotropic effects, velocity model heterogeneity, or both remains a key challenge. While reflection signatures may be insufficient for distinguishing these attributes, diffraction information in seismic datasets often provides richer insights into subsurface structures. In response to these challenges, we propose a framework that explores the feasibility of using diffraction traveltime parameters as indicators of anisotropy. By introducing an average measurement velocity derived from a cluster of diffraction traveltime responses, defined as a function of the traveltime slopes estimated from the dataset, we aim to discern the prevalence of anisotropy, heterogeneity, or both within a target region. Experiments conducted with synthetic data designed to simulate realistic scenarios have yielded promising results.

Keywords: diffraction velocity; anisotropy detection; heterogeneity; cluster of diffractions; seismic processing.

INTRODUCTION

Accurately characterizing subsurface geological structures is imperative for pinpointing hydrocarbon reservoir locations, and this task is often accomplished through a reliable seismic data processing framework (Yilmaz, 2001). However, inhomogeneous media, which result in velocity variations, pose an additional layer of complexity to this crucial endeavor. When such variations result from heterogeneity and anisotropy in the subsurface, the kinematic parameters used in the isotropic inversion procedure are subject to distortion due to the influence of anisotropic contributions, which results in non-physical inversion results.

Anisotropy influence in this context can stem from various factors, such as the intrinsic alignment of mineral grains in certain geological formations or fracture orientation. In the first condition, this alignment may be induced by thin isotropic layers with thicknesses smaller than the seismic wavelength. In the second condition, the orientation of fractures orientation within the subsurface, density, and connectivity can significantly influence the propagation of seismic waves, causing directional variations in seismic velocities. These anisotropic features can substantially impact the seismic wavefront kinematics, introducing intricacies that must be carefully considered in the characterization process (see Červený, 2001; Tsvankin, 2012, for more details).

In light of these conditions, meticulous analysis of how velocity variations influenced by anisotropy affect the kinematics of seismic waves becomes crucial. This analysis is essential for unraveling the complexities introduced by subsurface heterogeneities and ensuring the accuracy of the inversion process. By understanding how anisotropic contributions deform the wavefront propagation, interpreters can refine their models and enhance the precision of subsurface imaging, ultimately contributing to enhanced precision in decision-making in hydrocarbon exploration and reservoir delineation.

The characterization of transversely isotropic (TI) symmetries by parameters given by Thomsen (1986) made it possible to incorporate, in a simplified form, the extraction of anisotropy parameters into seismic data processing. After that, several works have proposed ways to extract such parameters through the analysis of seismic datasets, e.g., Alkhalifah (1997) presented a framework for a real field-data example that is based on reflections, and parameters are extracted using an offset-dependent nonhyperbolic traveltime. However, this procedure is only practical in anisotropic homogeneous media. When heterogeneity in the medium is considered, the *anellipticity* attribute η loses its kinematic interpretation and works as a best-fitting parameter (Bloot et al., 2018). Consequently, the result is a better stacking velocity than is estimated by the theoretical normal moveout velocity (V_{NMO}) in this case. Besides, by the normal incidence point (NIP) theorem (Hubral and Krey, 1980), V_{NMO} remains unaffected by the curvature of the reflector. Conversely, higher-order parameters are subject to such influences, potentially rendering the inversion of anisotropic parameters unreliable, even in a homogeneous medium. However, as for reflected waves, diffracted waves also have relevant information regarding the geological structure in the subsurface, with a notable advantage that the diffraction traveltime event as a whole is related to a single point in the subsurface. Therefore, determining the kinematic contributions for diffraction response is a topic of great interest, with applications varying from structural characterization to velocity analysis. Several authors have studied the use of diffractions in seismic processing (e.g., Landa and Keydar, 1998; Dell et al., 2013; Waheed et al., 2013; Gelius and Tygel, 2015; Faccipieri et al., 2016; Waheed et al., 2017; Coimbra et al., 2019). In general, the amplitude of diffracted waves is weaker than one of reflected waves. Such a feature makes the procedure of recovering diffraction responses from seismic data a really technical challenge.

In this study, we have investigated the practicality of using diffraction traveltime parameters as indicators of an anisotropy signature. Our research shows that it is feasible to identify a velocity signature by analyzing the attributes of slope and wavefront curvature from the diffraction traveltime. Additionally, our framework enables us to obtain signatures associated with anisotropy and lateral heterogeneity from the seismic dataset. It is worth noting that previous research, such as Alkhalifah and Tsvankin (1995), has demonstrated the possibility of transforming V_{NMO} into a slope function. Furthermore, understanding the specific type of anisotropy present in the medium is crucial to avoid employing inversion methods with excessive degrees of freedom. This knowledge prevents the problem from becoming underdetermined, mitigating the risk of multiple non-physical solutions arising for such a situation.

The proposed approach is valid for general and, specifically, for TI media. However, the vertical symmetry is of great interest for practical purposes (Alkhalifah, 1997); for this motive, the validation experiments have a focus in this case. Our synthetic experiments in vertical transversely isotropic (VTI) media show that the variation of the measured velocity is considerably small in the presence of pure vertical heterogeneity and has higher deviations in the presence of anisotropy. Based on this, we also determine an average velocity using a cluster of diffraction responses, which we refer to calculate if the medium has lateral velocity variations based on the direction (anisotropy) or position (lateral heterogeneity). The synthetic examples are designed to demonstrate two intrinsic aspects related to the presentation of this methodology. The first synthetic example is a model based on ray theory, which has all parameters well-controlled for selecting examples. In this scenario, the new approach is tested and is accurate for determining the correct tendency in the anisotropy parameter values (making them effective parameters). However, the corrected tendency is achieved if it is possible to isolate and select diffraction events near the target region. In the real case of seismic processing, extracting diffraction traveltime parameters becomes a complicated task. The seismic diffraction separation operator must work with the information the seismic section provides based on seismic response events, including information about reflection, diffraction, multiple events and noise. To extract the diffraction response, such an operator must prospect the data using tools based on coherence analysis and deal with all sorts of noises in the data. Based on this problem, we formulate a second synthetic example to evaluate the methodology in a more realistic scenario. Using complex velocity model benchmark data, a seismic section is generated through finite difference modeling. The model is designed to have a prevalence of heterogeneity with a target region containing VTI anomalies. Unlike the controlled case, in this scenario, the user must deal with the diffraction parameters it can extract from the data. The results have shown the technique effectiveness in determining the presence or absence of anisotropy in only the seismic response section. Finally, this approach can be incorporated into seismic processing as a tool for users to make decisions regarding the anisotropic signatures distorting the estimated wavefront curvature.

METHODOLOGY

In order to perform our analysis, we briefly describe the tool used to detect diffractions in a seismic-response dataset. Besides, we consider this dataset obtained along a single horizontal line with the midpoint and half-offset defined as (m, h) from which one can derive source-receiver coordinates. A supergather of source-receiver pairs is assumed to be arbitrarily lo-

cated concerning a reference pair $(m_0, 0)$, called the zero-offset (ZO) coordinates. Considering no prior knowledge about the subsurface geological structures, the challenge is to make the extraction of kinematic parameters with precision from the seismic data. For example, the tools given by Faccipieri et al. (2016) and Coimbra et al. (2019) can perform such parameter extraction. The traveltime approximation that describes the kinematics behind these cited operators can be described as

$$t_D(m,h) = \frac{1}{2}\left[\sqrt{(t_0 + A\Delta s)^2 + C(\Delta s)^2} + \sqrt{(t_0 + A\Delta r)^2 + C(\Delta r)^2}\right], \quad (1)$$

where $t_D(m,h)$ is the diffraction traveltime approximation, $\Delta s = \Delta m - h$, $\Delta r = \Delta m + h$, $\Delta m = m - m_0$, and t_0 is the two-way traveltime on the reference ray $(m_0, 0)$. Also, the traveltime parameter A is the slope of traveltime in the midpoint direction, and the traveltime parameter C can be viewed as a slowness squared, which can be specified in terms of derivatives of traveltime t as

$$A = \left.\frac{\partial t}{\partial m}\right|_{(m_0,0)}, \quad \text{and} \quad C = t_0 \left.\frac{\partial^2 t}{\partial h^2}\right|_{(m_0,0)}. \quad (2)$$

In practice, we can obtain the diffraction traveltime parameters of equation 1 through traveltime parameter search algorithms such as Ribeiro et al. (2023). Besides, as shown in Faccipieri et al. (2016), an optimal aperture in midpoints (based on the Fresnel zone) is necessary to achieve suitable results. Such parameters describe a time-migration velocity related to the points $(m_0, 0)$ in a ZO section, corresponding to the same point in depth.

In order to present an idea of the relationship between diffraction traveltime parameters and NMO velocity, we start with the following argument: in case we set $A = 0$ and $m = m_0$ in equation 1, we find the common-midpoint (CMP) moveout, which is given by

$$t_D(m_0, h) = t_{\mathrm{CMP}}(h) = \sqrt{t_0^2 + C_0 h^2}, \quad (3)$$

where we can interpret the parameter C_0 in terms of V_{NMO}, related to the phase vector arriving normal to the surface and measured as

$$C_0 = \frac{4}{[V_{\mathrm{NMO}}(0)]^2}. \quad (4)$$

The parameter C_0 represents a wavefront curvature measured with respect to the imaging ray (Hubral, 1983). Additionally, by equation 2, we can define the diffraction (D-) velocity, V_{D}, in the function of parameter A as (Coimbra et al., 2019)

$$\frac{4}{V_{\mathrm{D}}^2} = A^2 + C. \quad (5)$$

Thus, inverted in V_D, we have a D-velocity in function of A as

$$V_{\mathrm{D}}(A) = \frac{2V_{\mathrm{NMO}}(A)}{\sqrt{4 + A^2 V_{\mathrm{NMO}}^2(A)}}. \quad (6)$$

By measuring the D-velocity as a function of the kinematic parameter of the slope, we can extract meaningful information on the kinematic attributes of wavefront propagation. Furthermore, equation 6 describes such behavior of this velocity on the kinematic response of a diffraction wavefront. Even with such a velocity defined in the time domain, it is possible to relate this measurement velocity to its physical counterpart, which is given in terms of the phase velocity.

Diffraction-velocity variation in homogeneous media

Let us start our analysis with the simplest case of an isotropic homogeneous medium with constant velocity V_p. For this case, the physical interpretation of the kinematic parameter A is given by

$$A(\beta) = \frac{2\sin(\beta)}{V_p}, \quad (7)$$

where V_p is the vertical velocity of the P-wave, and β is the angle formed between the phase vector of the ray and the normal vector to the measurement surface at a midpoint m_0. Therefore, in this media, $V_{\mathrm{NMO}}(A(\beta))$ is given by

$$V_{\mathrm{NMO}}(A(\beta)) = \frac{2V_p}{\sqrt{4 - A^2(\beta)V_p^2}} = \frac{V_p}{\cos(\beta)}. \quad (8)$$

Replacing Equation 8 into Equation 6, we have $V_{\mathrm{D}}(A) = V_p$. This implies that the D-velocity is independent of A, indicating no velocity variation. Let us examine the VTI media for a homogeneous case considering the elliptic situation, i.e., the Thomsen parameters $\epsilon = \delta$. Following Alkhalifah and Tsvankin (1995) we have the exact expression for V_{NMO}, here in terms of A parametrized by β, given by

$$V_{\mathrm{NMO}}(A(\beta)) = \frac{2V_{\mathrm{NMO}}(0)}{\sqrt{4 - A^2(\beta)V_{\mathrm{NMO}}^2(0)}}, \quad (9)$$

with $V_{\mathrm{NMO}}(0) = V_p\sqrt{1 + 2\delta}$. Again, replacing equation 9 into equation 6, we have $V_{\mathrm{D}}(A) = V_{\mathrm{NMO}}(0)$, which implies that the D-velocity is constant along the diffraction response. Finally, we can collect the expressions and define the exact A and V_{NMO} expression, parametrized by β, for an anisotropic homoge-

neous medium given as follows (Tsvankin, 2012)

$$A(\beta) = \frac{2\sin(\beta)}{V(\beta)}, \quad \text{and}$$

$$V_{\text{NMO}}(A(\beta)) = \frac{V(\beta)}{\cos(\beta)} \left(\frac{\sqrt{1 + \frac{1}{V(\beta)} \frac{\partial^2 V}{\partial \beta^2}}}{1 - \frac{\tan(\beta)}{V(\beta)} \frac{\partial V}{\partial \beta}} \right), \quad (10)$$

where $V(\beta)$ is the phase velocity in function of β. It is known that the V_{NMO} estimated from reflection traveltimes recorded in common-midpoint geometry provides valuable information about the subsurface velocity field and anisotropic parameters (e.g., Alkhalifah and Tsvankin, 1995; Grechka and McMechan, 1996; Grechka and Tsvankin, 1998; Sadri and Riahi, 2010; Coimbra et al., 2023). However, with this information extracted from the CMP sections alone, it is hard to obtain a reliable inversion to extract such information. Therefore, using the NIP wavefronts, we can have V_{NMO} information for a set of arrival angles and thus extract a kinematic behavior from these wavefronts given by the variation of these angles.

Anisotropy characterization framework

In order to show how our anisotropy characterization works, it is essential to clarify the proposed procedure. The method is based on extracting the diffraction traveltime parameters from the seismic dataset with high precision through the diffracted wave separation procedure in a specific target region. Thus, the initial step involves implementing diffraction separation on the data using the tools outlined in Faccipieri et al. (2016) and Coimbra et al. (2019). These methods, designed for optimized diffraction separation, provide comprehensive information about D-velocity and slopes for each extracted diffraction response event. The panels containing this complete information are preserved after this initial processing step and can be utilized for various seismic processing objectives.

To enhance the redundancy of information about the target region, rather than analyzing each diffraction event individually, we opt for an analysis of clusters of diffraction responses. Once a specific cluster is defined, many D-velocity signatures as a slope function emerge. These individual signatures are stacked into a single average D-velocity measure.

Figure 1 illustrates the procedure for extracting information from the diffraction parameters in a selected target region. Let us explain how the diffraction responses can create the D-velocity function. Consider a region in a subsurface with N diffraction points. Each diffraction point has its response measured in a seismic dataset. After a process of diffraction event enhancement in such dataset, as mentioned before (see equation 1), it is obtained a parameter set as $\{A, C(A)\}_i$ for $i = 1, 2, \cdots, N$, which represents the set of slopes and curvature of the diffraction traveltime stored for each diffraction indexed by i at that region. Once we have the parameters obtained by the diffraction separation technique, we take an average of these parameters to construct the V_D in order to standardize the influence of the velocity variation due to heterogeneity in a way that does not destroy the anisotropy information. In mathematical terms, we can describe this operation as

$$V_D(A) = \frac{2}{N} \sum_{i=1}^{N} \left(A_i^2 + C_i(A_i) \right)^{-\frac{1}{2}}. \quad (11)$$

Besides, as the process is discrete and ordered, we can interpolate and extrapolate the parameters to leave them all on the same basis as the values of parameter A.

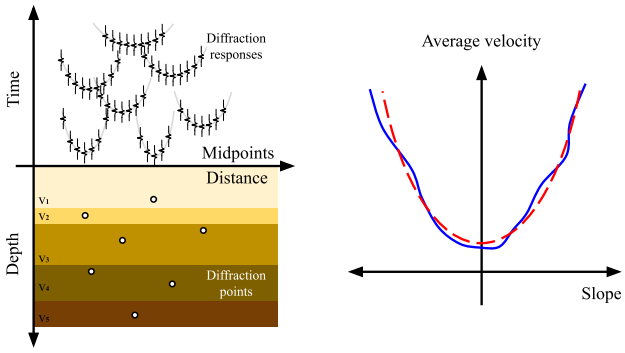

Figure 1: General illustration of the proposed framework applied to a target region showing the diffraction points in the depth domain and their respective ZO diffraction responses in the time domain, in which the gray lines represent the diffraction traveltime curves (left). The velocity and slope attributes picked over the diffraction responses at the region of interest create an average velocity response represented by the solid blue line. The best-fit velocity is represented by the red dashed line (right).

To obtain the average parameters of the medium, it is necessary to have a physical counterpart corresponding to some algebraic formula to extract useful information about the subsurface geology from the obtained velocity signature (for the target region) as illustrated in Figure 1. The analysis carried out for the homogeneous medium is now useful since, in that case, mathematical expressions are well-designed to connect the problem kinematics attributes with the medium phase velocity and the subsurface anisotropic parameters. Let us, therefore, introduce an ansatz for the measurement of D-velocity and make a search by these parameters through the following optimization problem

$$\Theta = \arg\min \left\| V_D(A) - \left[\frac{2V_{\mathrm{NMO}}(A)}{\sqrt{4 + A^2 V_{\mathrm{NMO}}^2(A)}} \right] (1 + \alpha A) \right\|, \tag{12}$$

where $\Theta = \{V_p, V_s, \epsilon, \delta, \alpha\}$ is the set parameter that makes up the medium with V_s being the S-wave velocity propagation. The introduction of the α-parameter works to detect middle to extreme lateral velocity variation cases.

In summary, the effectiveness of ansatz in describing anomalies in the data depends on the choice of V_{NMO}. For the TI media cases, equation 10 is used for our purposes. Another factor introduced into the ansatz is the search parameter α, which has a velocity dimension and is interpreted as a lateral velocity variation rate. Until now, no assumptions have been made about the nature of the model anisotropy. In the next section, the effectiveness of the ansatz is tested on some examples.

NUMERICAL RESULTS IN VTI MEDIA

In this numerical analysis section, we show the results for the specific case of VTI media. Two approaches were chosen to carry out the experiments. In the first one, the model was modeled using ray theory (Bloot et al., 2013); in the second, the model was created using the finite difference technique (Virieux, 1986). The procedures have a distinct explanatory nature. The ray-based models allow us to analyze the nature of the ansatz, described in the framework explanation, regarding its fidelity concerning contributions of anisotropy and inhomogeneity in the medium. In addition, the finite difference model is useful to illustrate the application of the proposed framework as a whole in a way that is closer to what would be done in a real data processing situation. The defined ansatz uses the exact squared phase velocity in VTI media (Tsvankin, 2012), which is given in terms of Thomsen's parameters as

$$V^2(\beta) = V_p^2 \left(1 + \epsilon \sin^2\beta - \frac{f}{2} + \frac{f}{2} \sqrt{1 + \frac{4\sin^2\beta}{f}(2\delta\cos^2\beta - \epsilon\cos 2\beta) + \frac{4\epsilon^2\sin^4\beta}{f^2}} \right), \tag{13}$$

where f is an auxiliary term described as

$$f = 1 - \frac{V_s^2}{V_p^2}. \tag{14}$$

To solve the optimization problem given by equation 12, we use the global optimizer differential evolution (Storn and Price, 1997) with a population of thirty individuals evolved by three hundred generations in all the experiments. Also, the crossover probability and the differential weight equal 0.7 and 0.9, respectively.

Ray model examples

In order to make a more refined experiment control, we consider two velocity models in the ray experiment with various ϵ and δ combinations. The ray tracing is based on the Eikonal given by Bloot et al. (2018), and, for our analysis, we use a second-order approximation in the parameter δ. The first model has vertical velocity variation defined as $V_p = 3292 + 0.7z$ [m/s]. The second model has a moderated lateral velocity variation, where $V_p = 3292 + 0.5x + 0.7z$ [m/s]. In both models, the S-wave velocity is $V_s = 1768$ [m/s]. In the context of the explained framework, we consider a cluster of diffraction responses near the target region to achieve suitable information redundancy. Figure 2 shows the diffraction point distribution and specifies the velocity model for the first scenario. The anisotropy model called Green River Shale (Thomsen, 1986) is considered for describing the medium, where $\epsilon = 0.195$ and $\delta = -0.220$; the performance of fitting of the proposed ansatz with respect to the diffraction cluster presented in Figure 2 is shown in Figure 3. For this example, $\alpha \approx 0$ is expected since no lateral velocity variation exists. Furthermore, the estimated anisotropic parameters are $\epsilon_E = 0.2163$ and $\delta_E = -0.1214$, which are not the exact values. However, they indicate the correct tendency of anisotropy contamination on the V_D function.

In addition, to analyze the V_D signature, the pure heterogeneous case was studied with $\epsilon = \delta = 0$ in the velocity model given by Figure 2. The result is shown in Figure 4, where the lateral velocity variation is irrelevant. This velocity behavior follows the pattern observed in a homogeneous medium with constant velocities.

Considering the velocity model of the first scenario, let us move to a case where the anisotropy parameters are not constant. Let us consider a different model where the medium is isotropic at depths from measurement surface to 1000 [m] and the Green River Shale at depths from 1000 [m] to 2000 [m]. In this case, we first consider the diffraction cluster with the same structure as the previous example. The result is illustrated in Figure 5; the estimated anisotropic parameters are $\epsilon_E = 0.1634$ and $\delta_E = 0.1081$ with $V_s = 1761.5$ [m/s] and $V_p = 3157.6$ [m/s]. For this case, $\alpha = -0.0206$ [m/s] indicates no significant lateral variation with the position. However, the estimated anisotropy parameters do not represent the correct tendency concerning the medium real physics. Considering that the diffractions are spread between the isotropic and anisotropic target regions, it is clear that the estimated average velocity overlapped contributions from both cases. Besides, the velocity signature shown in Figure 5 highlights a small variation in the velocity, leading us to conclude that the isotropic part of the model heavily contaminates it.

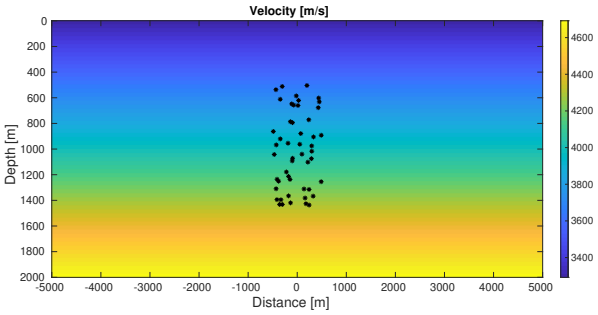

Figure 2: A cluster of diffraction points represented by the black asterisks in a heterogeneous medium with velocities $V_p = 3292+0.7z$ [m/s] and $V_s = 1768$ [m/s]. A similar cluster configuration is considered for other velocity backgrounds.

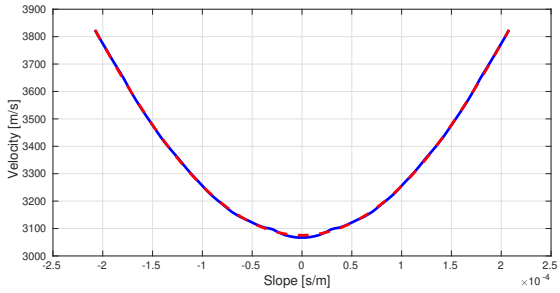

Figure 3: Average D-velocity response (solid blue line) of a diffraction cluster embedded in the VTI medium with $\epsilon = 0.195$, $\delta = -0.220$ and velocity described in Figure 2. The red dashed line represents the best-fitting parameters using equation 12. The estimated anisotropic parameters are $\epsilon_E = 0.2163$ and $\delta_E = -0.1214$.

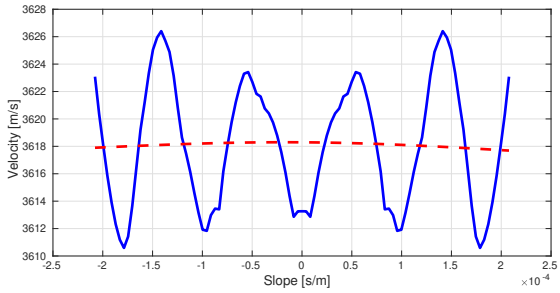

Figure 4: Average D-velocity response (solid blue line) of a diffraction cluster embedded in an isotropic medium with the velocity described in Figure 2. The red dashed line represents the best-fitting parameters using equation 12. The estimated anisotropic parameters are $\epsilon = -0.0083$ and $\delta = -0.0081$ which are not the exact values with $V_v = 1761.5$ [m/s] and $V_p = 3157.6$ [m/s]. For this case, $\alpha = -0.1378$ [m/s] indicates no lateral variation with position. Note that the velocity variation for this case is quite small.

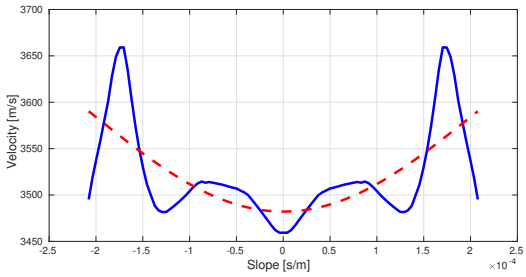

Figure 5: Average D-velocity response (solid blue line) of a diffraction cluster embedded in the VTI medium where the first half is isotropic and the second half is the Green River Shale model. The velocity model is described in Figure 2. The red dashed line represents the best-fitting parameters using equation 12.

Let us consider a compact diffraction cluster in the anisotropic part of the model. Such a situation can help unravel the correct structure and the propensity of the anisotropy contamination on velocity in that target region. The result is shown in Figure 6 for such a setting. The estimated anisotropic parameters are $\epsilon_E = 0.0806$ and $\delta_E = -0.1108$ which are not the exact values with $V_s = 1969.3$ [m/s] and $V_p = 3917.5$ [m/s]. For this case, $\alpha = 1.41$ [m/s] indicates no significant lateral variation with position. However, the estimated effective parameter values follow the subsurface anisotropic structure.

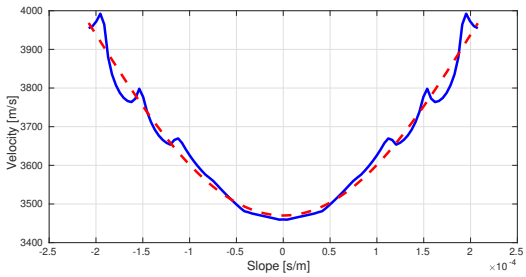

Figure 6: Average D-velocity response (solid blue line) of a diffraction cluster (extracted in the anisotropic target region) embedded in the VTI medium where the first half is isotropic and the second half is the Green River Shale model. The velocity model is described in Figure 2. The red dashed line represents the best fitting using equation 12.

As we can see in the previous results, the lateral variation detected at the D-velocity is induced by the influence of the anisotropy parameters on the wave propagation in the subsurface. Now consider the second scenario illustrated in Figure 7. In this model, the P-velocity varies laterally with the position and anisotropy when we consider the same constant model with $\epsilon = 0.195$ and $\delta = -0.220$ as the previous example. The result is illustrated in Figure 8. The estimated anisotropic parameters are $\epsilon_E = 0.1255$ and $\delta_E = -0.1876$ and $V_p = 3920.5$ [m/s], $V_s = 1993.7$

[m/s] and $\alpha = 770.3$ [m/s], which are not the exact values. However, again, they indicate the correct tendency of anisotropy contamination in V_D for such a medium. The presence of anisotropy curves the D-velocity response. In the case of pure heterogeneity, the response is almost flat, as shown in Figure 9. Note that the extracted parameter can be refined by introducing more diffractions.

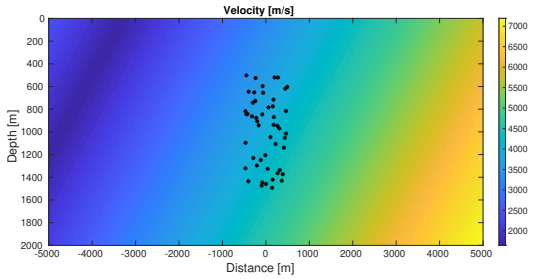

Figure 7: Cluster of diffraction points represented by the black asterisks in a heterogeneous medium with velocities $V_p = 3292 + 0.5x + 0.7z$ [m/s] and $V_s = 1768$ [m/s].

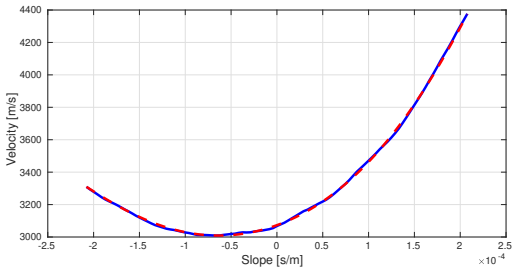

Figure 8: Average D-velocity response (solid blue line) of a diffraction cluster embedded in the VTI medium with $\epsilon = 0.195$, $\delta = -0.220$ and velocity described in Figure 7. The red dashed line represents the best fitting using equation 12.

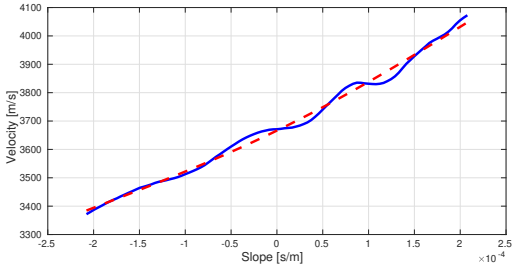

Figure 9: Average D-velocity response (solid blue line) of a diffraction cluster embedded in an isotropic medium with the velocity described in Figure 7. The red dashed line represents the best fitting using equation 12. The estimated anisotropic parameters are $\epsilon_E = 0.0672$ and $\delta_E = 0.0510$ which are not the exact values with $V_s = 1006.5$ [m/s] and $V_p = 3476.8$ [m/s]. For this case, $\alpha = 394.41$ [m/s] indicates lateral variation with the position.

Finite Difference model example

In order to evaluate the proposed framework on a challenging and realistic scenario, we simulate a dataset using the second-order finite-difference method that discretizes the elastic equation following the reference equation given by Virieux (1986). For modeling purposes, we modify the BP model (Billette and Brandsberg-Dahl, 2005). Figure 10 illustrates the P-wave velocity model discretized at 6 [m] intervals, encompassing 1396 x 1200 grid points. We set the vertical S-wave velocity as $V_s = V_p/2$ and density $\rho = 1$. Figures 11 and 12 depict the Thomsen's parameter, i.e., δ and ϵ, respectively. The dataset was generated with 601 sources and 601 receivers arranged in a split spread geometry, starting with the first pair located at 900 [m] and spaced at 12 [m]. The maximum recording time is 6 [s], sampled at 1 [ms] intervals. Figure 13 displays the ZO section. This section allows us to observe the reflections of the VTI medium anomaly event, along with the inclusion of additional diffraction events. Moreover, it showcases interface diffraction events resulting from the numerical method mesh.

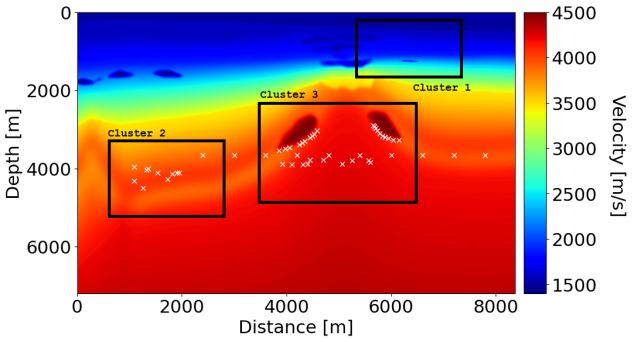

Figure 10: P-wave velocity (BP model). The white times (×) indicate the diffraction points added to the model to validate the proposed method. The regions in the boxes contain the clusters of the target regions where diffractions were picked for the experiments.

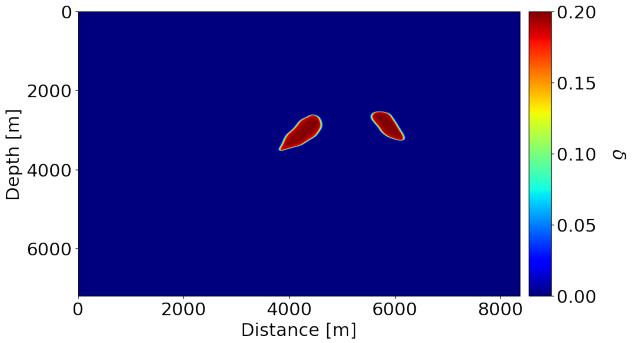

Figure 11: Thomsen's δ parameter simulated in the model depicted in Figure 10.

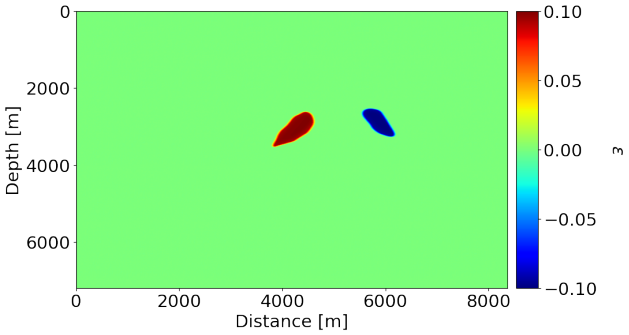

Figure 12: Thomsen's ϵ parameter simulated in the model depicted in Figure 10.

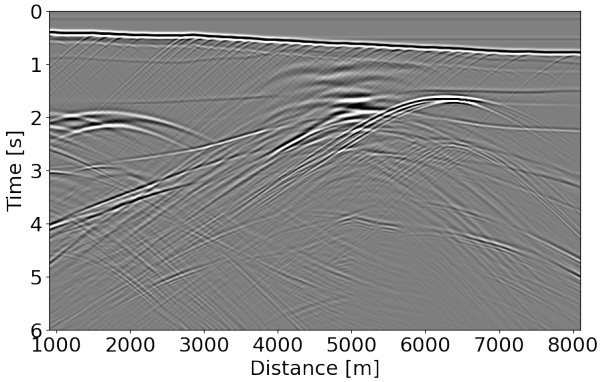

Figure 13: ZO section obtained through finite differences modeling considering the velocity model and Thomsen's parameters shown in Figures 10, 11 and 12.

Detecting the presence or absence of anisotropy begins with collecting the diffraction section as illustrated in Figure 13; strong reflection events may mask the diffracted information. In the first step, it is necessary to apply the diffraction-traveltime separation to obtain a section where the diffractions are enhanced. Therefore, we apply a diffraction separation process following the steps described by the US Patent Application (Mundim et al., 2024), which includes a preconditioning step to attenuate reflections and a diffraction enhancement through a diffraction-traveltime approximation. For the preconditioning step, we use midpoint and offset window-aperture sizes of 100 [m] and 50 [m], respectively, with a 75 [m] spreading aperture in the midpoint direction. For the application of diffraction enhancement, time-varying estimation apertures were considered. In the midpoint direction, window apertures rang up to 500 [m] at one second, increasing linearly to 1000 [m] at two seconds; in the offsets, we have 1000 [m] at one second and 2000 [m] at two seconds. For the diffraction operator stacking process, apertures ranged from 50 [m] at 0.1 [s], increasing linearly to 800 [m] at five seconds; in the offsets, we have 100 [m] at 0.1 [s] and 1800 [m] at five seconds. The diffraction spreading considers window apertures of 500 [m] at 0.1 [s], increasing to 1000 [m] at five seconds (see Coimbra et al., 2016, 2019, for more details about such operators).

In the second step, we determine regions where we collect the diffractions to construct the D-velocity function. We use the D-velocity and slope panels given in Figures 14 and 15 to achieve this objective. The third and crucial step is determining the regions of interest with plenty of diffraction information to be used. Models based on the finite difference technique typically present diffraction events with low smoothing in the presence of data. Despite this, we introduce additional diffraction events close to regions with great depth and below the salt structure. Three areas of interest with diffraction events are selected and named Clusters 1, 2 and 3, respectively.

Cluster 1 is selected through diffractions generated by the finite difference in the shallowest regions. We can use this case to perform a validation test in a shallow region without anisotropy. The panels for this case are illustrated in Figures 16 and 17. For this case, Figure 22 shows the D-velocity functions with extracted parameters $V_p = 1807.2$ [m/s], $V_s = 904.6$ [m/s], $\epsilon = \delta = 0$ and $\alpha = 0$ [m/s]. The result follows what is expected for the target region with small velocity variation, no lateral velocity variation, and, consequently, a prevalence of vertical heterogeneity at that region (see Figure 10).

Cluster 2 is selected through diffractions at the region illustrated in Figure 10 with velocity and slope panels given in Figures 18 and 19. For this case, the D-velocity functions are showed in Figure 23 with extracted parameters $V_p = 2094.9$ [m/s], $V_s = 1118.3$ [m/s], $\epsilon_E = -0.0072$, $\delta_E = 0.0005$ and $\alpha = -6.0149$ [m/s]. The method detects low lateral velocity variation. The values of ϵ_E and δ_E indicate a negligible amount, helping the interpretation to conclude that the environment has a prevalence of heterogeneity and no anisotropy.

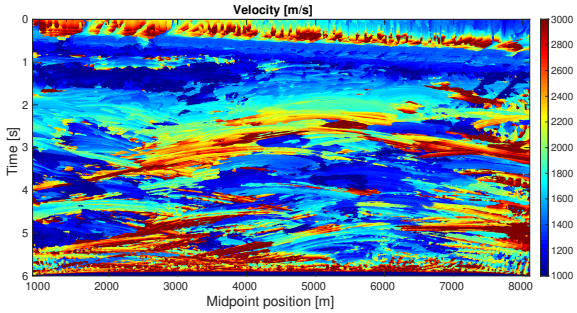

Figure 14: Estimated velocities related to diffraction responses obtained by the diffraction traveltime (equation 1).

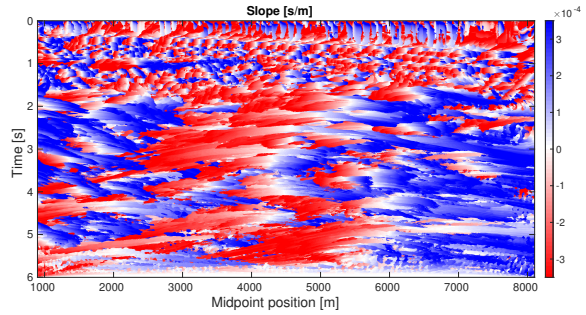

Figure 15: Estimated slopes related to diffraction responses obtained by the diffraction traveltime (equation 1).

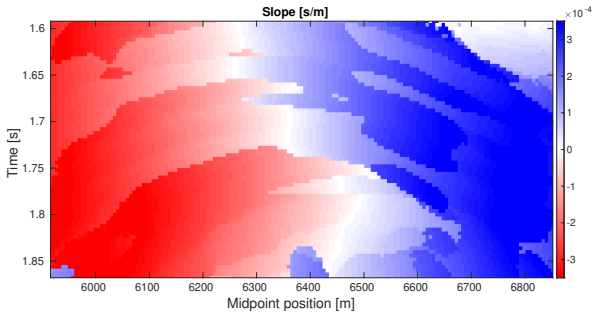

Figure 16: Cluster 1 - Detailed view of the estimated slopes

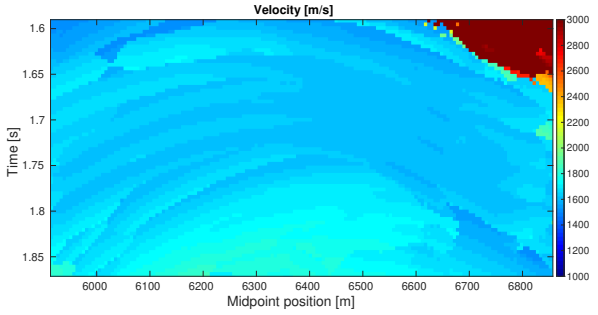

Figure 17: Cluster 1 - Detailed view of the estimated velocities.

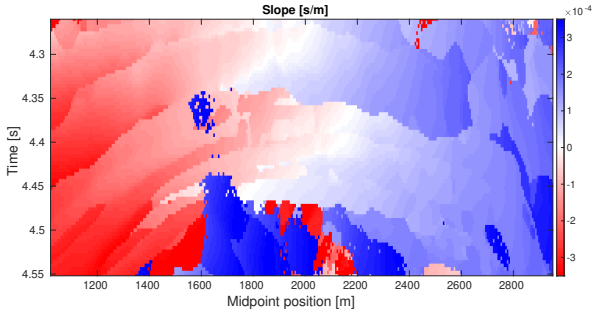

Figure 18: Cluster 2 - Detailed view of the estimated slopes.

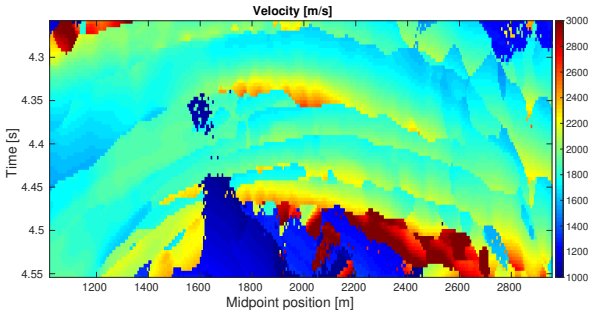

Figure 19: Cluster 2 - Detailed view of the estimated velocities.

Cluster 3 is selected through diffractions at the region illustrated in Figure 10 with velocity and slope panels given in Figures 20 and 21. Figure 24 shows the D-velocities, which are obtained the parameters $V_p = 1581.7$ [m/s], $V_s = 1705.8$ [m/s], $\epsilon_E = 0.2996$, $\delta_E = -0.1176$ and $\alpha = -327.5255$ [m/s] representing the tendency detected by the method. This region is of great interest, and the anisotropy contamination on the estimated D-velocity function is expected to be detected. Unlike the other two cases, in this target, we can see a pronounced variation in the average velocity following a pattern identical to the results studied in the examples modeled by ray theory when anisotropy is considered. Furthermore, we obtain values for the anisotropy and lateral velocity parameters using the ansatz. Even without knowledge of the subsurface, a user can conclude that lateral velocity variation is simultaneously induced by heterogeneity and anisotropy in this region.

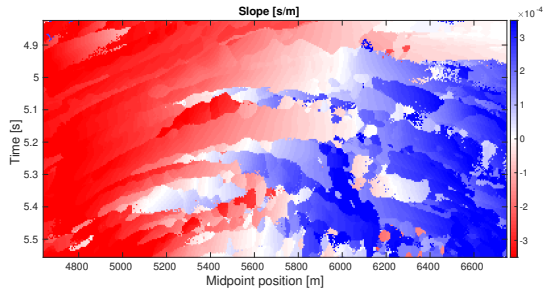

Figure 20: Cluster 3 - Detailed view of the estimated slopes.

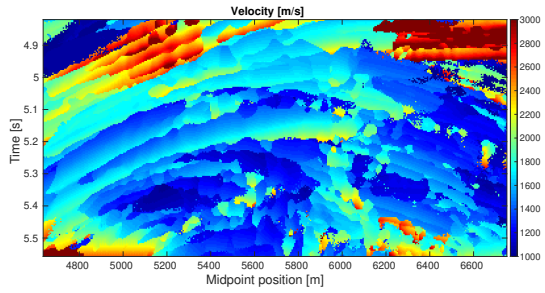

Figure 21: Cluster 3 - Detailed view of the estimated velocities.

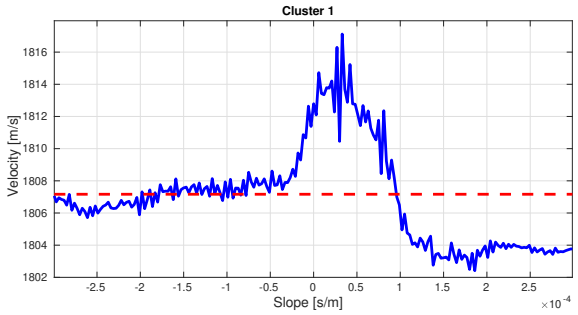

Figure 22: Cluster 1 - Average D-velocity response (solid black line) of the diffraction cluster embedded in the VTI medium. The red dashed line represents the best-fitting parameters using equation 12.

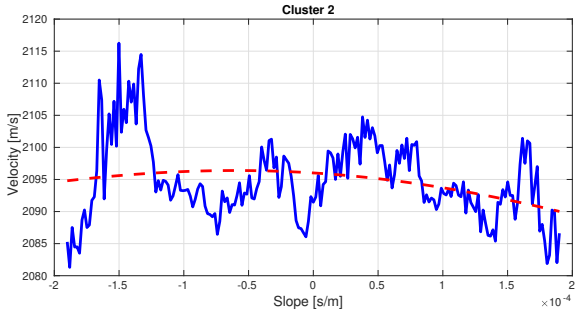

Figure 23: Cluster 2 - Average D-velocity response (solid black line) of the diffraction cluster embedded in the VTI medium. The red dashed line represents the best-fitting parameters using equation 12.

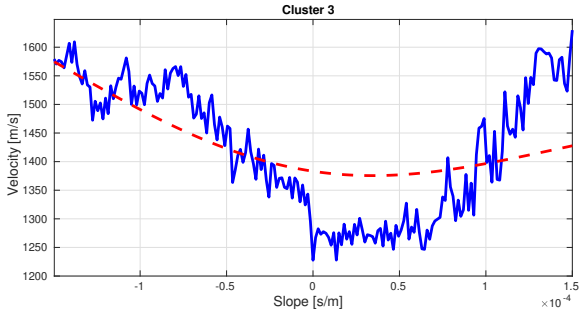

Figure 24: Cluster 3 - Average D-velocity response (solid black line) of the diffraction cluster embedded in the VTI medium. The red dashed line represents the best-fitting parameters using equation 12.

DISCUSSION

Detection of local heterogeneities was initially proposed in Landa and Keydar (1998) for an isotropic context and in a very distinct approach in comparison with our proposed framework. Some authors also used diffractions and tried to estimate anisotropic parameters from Diffraction traveltime curves with complex expressions modeled in terms of physical attributes of the medium (see, e.g., Dell et al., 2013; Waheed et al., 2013). However, in the presence of complex models, the anisotropic parameters may be very sensitive, resulting in best-fit parameters, which do not necessarily mean best-inversion parameters in some cases. Waheed et al. (2017) proposed a method to perform the inversion using diffractions and an effective parameter η in a Dix-type procedure (Dix, 1955). One of this approach drawbacks is assuming the knowledge of vertical velocity, V_p, what we know does not occur in practice. On the other hand, any Dix-type procedure in any isotropic and anisotropic medium is subject to the effects of the velocity spread factor (e.g., Cameron et al., 2007; Coimbra et al., 2023). Our proposal presents a framework that can be incorporated into seismic processing, allowing the user to interpret whether or not the medium has the presence of anisotropy.

Furthermore, a user must make decisions based exclusively on the seismic data section in real seismic processing situations. With the increasing complexity of regions with hydrocarbon reserves, the velocity analysis with purposes of inversion demands more knowledge and information about subsurface attributes, and the data given in Figure 13 are the only information about the subsurface in practical scenarios. On the other hand, our analysis using models based on Ray Theory allows a robust understanding concerning the ansatz behavior and efficiency in heterogeneous cases. Moreover, the examples demonstrated in the section based on ray theory allow us to conclude that if we have localized diffractions around the target with anisotropy, then a reasonable estimate can be made about effective ϵ and δ.

Unfortunately, the real cases are similar to the case where it is necessary to prospect diffractions in the data to be able to determine target regions that may not, in principle, be adequate for parameter search purposes. However, this calculation indicates if the medium has lateral velocity variations based on the direction (anisotropy contamination) or position (pure heterogeneity). In this more realistic case, the anisotropy parameters obtained indicate that the presence of anisotropy is evident and delimit this region as a target for more detailed analysis when the migration and inversion procedures are performed. Furthermore, such parameters may indicate the presence of oriented fractures.

One bottleneck is relative to D-velocity and slope panels, extracted in a tool well-designed to optimize the Semblance function, best to achieve redundancy and collect the diffraction; achieving the best diffraction traveltime parameters is not the main purpose. To get suitable kinematic parameters, an additional procedure must be incorporated into this framework in future research to complement the diffraction section with well-accurate kinematic parameters.

CONCLUSIONS

In summary, our novel approach addresses the challenge of identifying anisotropy and pure heterogeneity in subsurface media during seismic processing. Lateral velocity variations and anisotropic contributions can introduce inaccuracies in velocity inversion, imaging and data interpretation, affecting the quality of seismic dataset procedures. Our proposal utilizes diffraction traveltime parameters as indicators to discern the prevalence of anisotropy or pure heterogeneity. Tested on synthetic examples, our framework offers potential integration into seismic processing as an auxiliary tool for decision-making on geological structure features. The robustness of our approach, demonstrated in tests with a substantial number of diffractions, enables the estimation of effective anisotropy parameters. Despite its validity in VTI media, further research will refine the approach for more complex anisotropy models.

ACKNOWLEDGMENTS

The authors thank British Petroleum and Frederic Billette for providing the BP Benchmark and Shearwater GeoServices for the Reveal academic licence. The authors also thank the High-Performance Geophysics Laboratory (HPG Lab) team and Petróleo Brasileiro S.A. (Petrobras) for all the support.

DATA AND MATERIALS AVAILABILITY

Data associated with this research and additional information can be obtained from the corresponding author.

REFERENCES

Alkhalifah, T., 1997, Velocity analysis using nonhyperbolic moveout in transversely isotropic media: Geophysics, **62**, 1839–1854, doi: 10.1190/1.1444285.

Alkhalifah, T., and I. Tsvankin, 1995, Velocity analysis for transversely isotropic media: Geophysics, **60**, 1550–1566, doi: 10.1190/1.1443888.

Billette, F., and S. Brandsberg-Dahl, 2005, The 2004 BP velocity benchmark: Presented at the 67th EAGE Conference & Exhibition, European Association of Geoscientists & Engineers, Madrid, Spain. doi: 10.3997/2214-4609-pdb.1.b035.

Bloot, R., T. A. Coimbra, J. H. Faccipieri, and M. Tygel, 2018, Common-reflection-surface method in weakly anisotropic vertical transverse isotropic media: Geophysics, **83**, C99–C113, doi: 10.1190/geo2017-0368.1.

Bloot, R., J. Schleicher, and L. T. Santos, 2013, On the elastic wave equation in weakly anisotropic VTI media: Geophysical Journal International, **192**, 1144–1155, doi: 10.1093/gji/ggs066.

Cameron, M. K., S. B. Fomel, and J. A. Sethian, 2007, Seismic velocity estimation from time migration: Inverse Problems, **23**, 1329–1369, doi: 10.1088/0266-5611/23/4/001.

Červený, V., 2001, Seismic ray theory: Cambridge University Press, 722 pp, doi: 10.1017/cbo9780511529399.

Coimbra, T. A., R. Bloot, and J. H. Faccipieri, 2023, Exploring velocity-spreading factor and consequences through dynamic ray-tracing in general anisotropic media: A comprehensive tutorial: `arXiv:2304.02069v1 [physics.geo-ph]`, doi: 10.48550/arXiv.2304.02069.

Coimbra, T. A., J. H. Faccipieri, J. H. Speglich, L.-J. Gelius, and M. Tygel, 2019, Enhancement of diffractions in prestack domain by means of a finite-offset double-square-root traveltime: Geophysics, **84**, V81–V96, doi: 10.1190/geo2018-0160.1.

Coimbra, T. A., A. Novais, and J. Schleicher, 2016, Offset-continuation stacking: Theory and proof of concept: Geophysics, **81**, V387–V401, doi: 10.1190/geo2015-0473.1.

Dell, S., A. Pronevich, B. Kashtan, and D. Gajewski, 2013, Diffraction traveltime approximation for general anisotropic media: Geophysics, **78**, WC15–WC23, doi: 10.1190/geo2012-0346.1.

Dix, C. H., 1955, Seismic velocities from surface measurements: Geophysics, **20**, 68–86, doi: 10.1190/1.1438126.

Faccipieri, J. H., T. A. Coimbra, L. J. Gelius, and M. Tygel, 2016, Stacking apertures and estimation strategies for reflection and diffraction enhancement: Geophysics, **81**, V271–V282, doi: 10.1190/GEO2015-0525.1.

Gelius, L.-J., and M. Tygel, 2015, Migration-velocity building in time and depth from 3D (2D) Common-Reflection-Surface (CRS) stacking - theoretical framework: Studia Geophysica et Geodaetica, **59**, 253–282, doi: 10.1007/s11200-014-1036-6.

Grechka, V., and I. Tsvankin, 1998, Feasibility of nonhyperbolic moveout inversion in transversely isotropic media: Geophysics, **63**, 957–969, doi: 10.1190/1.1444407.

Grechka, V. Y., and G. A. McMechan, 1996, 3-D two-point ray tracing for heterogeneous, weakly transversely isotropic media: Geophysics, **61**, 1883–1894, doi: 10.1190/1.1444103.

Hubral, P., 1983, Computing true amplitude reflections in a laterally inhomogeneous earth: Geophysics, **48**, 1051–1062, doi: 10.1190/1.1441528.

Hubral, P., and T. Krey, 1980, Interval velocities from seismic reflection time measurements: Society of Exploration Geophysicists, Tulsa, Oklahoma, 214 pp, doi: 10.1190/1.9781560802501.

Landa, E., and S. Keydar, 1998, Seismic monitoring of diffraction images for detection of local heterogeneities: Geophysics, **63**, 1093–1100, doi: 10.1190/1.1444387.

Mundim, E. C., C. Benedicto, J. H. Faccipieri Jr.,

D. R. Serrano, M. Tygel, and T. A. A. Coimbra, 2024, Method for separating information associated with diffraction events from specular information present in the seismic data: U.S. Patent App. 18/365,795. (US 2024/0045090 A1).

Ribeiro, J., N. Okita, T. A. Coimbra, and J. H. Faccipieri, 2023, Ultra-fast traveltime parameters search by a coevolutionary optimization approach using graphics processing units: `arXiv:2304.11399v1 [physics.geo-ph]`, doi: 10.48550/arXiv.2304.11399.

Sadri, M., and M. A. Riahi, 2010, Ray tracing and amplitude calculation in anisotropic layered media: Geophysical Journal International, **180**, 1170–1180, doi: 10.1111/j.1365-246x.2009.04464.x.

Storn, R., and K. Price, 1997, Differential Evolution - A Simple and Efficient Heuristic for Global Optimization over Continuous Spaces: Journal of Global Optimization, **11**, 341–359, doi: 10.1023/a:1008202821328.

Thomsen, L., 1986, Weak elastic anisotropy: Geophysics, **51**, 1954–1966, doi: 10.1190/1.1442051.

Tsvankin, I., 2012, Seismic signatures and analysis of reflection data in anisotropic media, Third edition: Society of Exploration Geophysicists, Tulsa, Oklahoma, 459 pp, doi: 10.1190/1.9781560803003.

Virieux, J., 1986, P-SV wave propagation in heterogeneous media: Velocity-stress finite-difference method: Geophysics, **51**, 889–901, doi: 10.1190/1.1442147.

Waheed, U. b., T. Alkhalifah, and A. Stovas, 2013, Diffraction traveltime approximation for TI media with an inhomogeneous background: Geophysics, **78**, WC103–WC111, doi: 10.1190/geo2012-0413.1.

Waheed, U. b., A. Stovas, and T. Alkhalifah, 2017, Anisotropy parameter inversion in vertical axis of symmetry media using diffractions: Geophysical Prospecting, **65**, 194–203, doi: 10.1111/1365-2478.12417.

Yilmaz, O., 2001, Seismic data analysis: Processing, inversion, and interpretation of seismic data: Society of Exploration Geophysicists, Tulsa, Oklahoma, 2065 pp, doi: 10.1190/1.9781560801580.

Coimbra, T.A.A.: conceptualization, writing-original draft preparation, review and editing; **Bloot, R.**: conceptualization, writing-original draft preparation, review and editing; **Camargo, A.W.**: conceptualization, writing-original draft preparation, review and editing; **Faccipieri Junior, J.H.**: conceptualization, writing-original draft preparation, review and editing.

Received on December 16, 2023 / Accepted on May 14, 2024